Variable Connectivity Method for the Atomistic Monte Carlo Simulation of Polydisperse Polymer Melts

P. V. Krishna Pant†

Department of Chemical Engineering, University of California, Berkeley, Berkeley, California 94720-1462

Doros N. Theodorou*

Department of Chemical Engineering, University of Patras, GR-26500 Patras, Greece, and Molecular Modelling of Materials Group, National Research Centre for the Physical Sciences "Demokritos", GR-15310 Ag. Paraskevi, Athens, Greece

Received April 18, 1995®

ABSTRACT: A new Monte Carlo algorithm for the simulation of atomistically detailed polymer melts is presented. The method introduces connectivity relationships as variables in the description of the polymer. The connectivity of the polymer is altered in Monte Carlo moves that satisfy the detailed constraints of molecular geometry. Connectivity-altering moves are seen to induce large jumps in the configuration space of the bulk polymer, thereby greatly enhancing the efficiency with which molecular configurations are sampled. Simulations are carried out in a *semigrand* ensemble in which the chain length distribution is controlled by a spectrum of chemical potentials. Limiting chain length distributions are derived and compared with simulation results. Volumetric and structural predictions of the method are found to be in agreement with previous work.

1. Introduction

Molecular simulations have been successful in elucidating several aspects of the dynamic, structural, and thermodynamic properties of polymer melts over the past decade.[1,2] This has been made possible, in part, by the increasing diversity and sophistication of simulation methodology, which has come to encompass a wide range of dynamic and statistical-mechanical approaches. In particular, *molecular dynamics* (MD) algorithms, which track the temporal evolution of a molecular system under the influence of interatomic forces, have found the widest application: in examining chain dynamics,[3−7] in studies of the glass transition,[8−10] in predictions of the diffusion of gaseous penetrants through polymer melts,[11−13] and in several other phenomena.

Much attention has also been focused on predicting the time-averaged (or *ensemble-averaged*) thermodynamic properties of polymer melts. Being simple and generally applicable, MD has found application to this class of problems as well, such as in studies of their volumetric behavior.[8,14] However, an adequate computation of thermodynamic averages demands a robust sampling of structural fluctuations in the bulk polymer. In this respect, the dynamic approach has not been entirely successful—despite major advances, MD simulations have not proved adequate for the thermal equilibration of long-chain melts.[15,16] MD studies of polymer melts must rely, therefore, on the generation of initial structures that are close to thermal equilibrium, which for melts of long chains is in itself a complex problem. The cause for this predicament is that the longest relevant relaxation time of a chain molecule rises rapidly with chain length, making the equilibration times of entangled, truly polymeric systems inaccessible in dynamic simulations.

In parallel with MD, considerable progress has been made in the development of Monte Carlo (MC) simulation methods for amorphous polymers. MC simulations proceed by generating a Markov chain of configurations that samples the probability distribution of the statistical-mechanical ensemble of interest. At each iteration, a change in some (typically small) subset of the atomic coordinates is attempted; the disordering move is accepted with a probability given by the Metropolis rules.[17] In contrast with MD, the moves may be tailored to achieve efficient sampling. Over the years, several moves specific to chain molecules have been developed and employed effectively in simulations, including reptation,[18,19] continuum configuration bias,[20−22] and concerted rotation.[23−25] The first two of these accelerate the diffusion of the center of mass of the chain, while the last improves the sampling of local fluctuations in chain structure. More recently, hybrid Monte Carlo methods[26] have been employed in polymer melt simulations.[15,27] In these, a single Monte Carlo move consists of a short dynamic trajectory. The dynamic integrator is required to be time-reversible and area-preserving in phase space. These requirements, satisfied by simple integrators such as the *leapfrog* algorithm, ensure the microscopic reversibility of the MC-generated Markov chain of states for arbitrarily large integration steps. Deviations in energy over the length of each dynamic trajectory depend on the integration time step chosen, and moves are accepted or rejected in accordance with the usual Metropolis rules. This allows, in general, for the use of somewhat larger time steps than permissible in molecular dynamics, with no loss of rigor. However, even these methods are seen to fail in equilibrating melts of chains longer than 70 methylene units.[15]

In principle, MC moves can be made to tunnel through energetic barriers in the configurational space of the polymer, circumventing the limitations of dynamic algorithms. This feature has been exploited within lattice polymer simulations in moves that alter chain connectivity,[28−30] greatly enhancing the sampling efficiency. Such moves allow for structural fluctuations in highly dense lattice polymers, which cannot thermally equilibrate by other means. They have also been employed effectively in simple off-lattice models.[31] The

† Present address: 1776 Building, M. E. Pruitt Research Center, The Dow Chemical Co., Midland, MI 48674.

® Abstract published in *Advance ACS Abstracts,* August 1, 1995.

0024-9297/95/2228-7224$09.00/0

appeal of such moves is readily apparent: small alterations to the connectivity result in large jumps in the configuration space of the polymer, especially accelerating the rate of evolution of long-range structural features such as the end-to-end vector of the chain.

In the present work, changes to connectivity relationships are introduced to the simulation of atomistically detailed polymer models. A simple example of such a model, which was used here as a test case, is described in section 2. In this case, the implementation is complicated by the constraints of molecular geometry: the specification of all relevant bond lengths and angles requires, in general, that three atoms be moved together to effect a change in connectivity. The geometric problem of *bridging* a pair of dimers with a trimer, given all intervening bond lengths and angles, forms the basis of our implementation of the new MC moves. The objective is to exploit the flexibility of the Monte Carlo approach by designing moves that tunnel through energetic barriers in the polymer, enabling a robust exploration of its configuration space. This, in turn, holds promise for efficient, reliable predictions of the ensemble-averaged properties of dense chain-molecular systems.

To ensure microscopic reversibility, care must be taken to evaluate all the solutions of the geometric problem associated with the connectivity-altering move. The transformation of coordinates inherent in the execution of such moves subject to geometric constraints necessitates the incorporation of appropriate Jacobians of transformation[23,24] into the acceptance criteria. Further, the mechanism of site selection introduces biases that must correctly be accounted for in the acceptance criterion. These considerations are detailed in section 3. Tests of the validity of the algorithm are described in section 5.

Changes in connectivity introduce polydispersity into the simulated polymer, which is treated through the use of a *semigrand* ensemble, analogous to the ensembles of Briano and Glandt[32] and Kofke and Glandt.[33] A spectrum of chemical potentials controls fluctuations in the molecular weight distribution of the system.[34] Simple limiting distributions are derived in section 4 and compared with the results of simulations in section 5.

An alternate implementation of the geometric *bridge* is also presented in section 3, consisting of an iterative solution of the linearized constraint equations. This solution finds convenient application in MC moves akin to the *concerted rotation*.[23] In this case, the bonds penultimate to the bridge are rotated by a small amount and then rebridged, inducing local fluctuations in the structure. The rebridging is performed using an iterative Newton–Raphson solution of the geometric constraints, starting from the unperturbed coordinates of the bridge.

The purpose of the present work is primarily to demonstrate the validity and efficiency of the new simulation technique. The method has been implemented on a simple model of polyethylene that has been studied previously via other methods.[23] This has allowed for direct comparisons of predicted structure and volumetric behavior, as well as of the efficiency of the algorithm, against previous work. These comparisons, for which the new moves are combined with reptations and volume fluctuations, are detailed in section 6.

2. Molecular Model

The molecular model used in this work is identical to that employed in our previous simulations of polyethylene.[23,25] Bond lengths and angles are constrained to their average values of 1.54 Å and 112°, respectively. For intramolecular interactions between segments separated by more than three atoms along the chain, and for all intermolecular interactions, methylene groups are treated as united Lennard-Jones force centers with a diameter σ of 3.94 Å and a well-depth ϵ of 0.098 kcal/mol. The Ryckaert–Bellemans torsional potential[35] is employed. Since the prime objective of this work is to present, validate, and evaluate the efficiency of a new simulation technique, the issue of refining potential parameters, both for the nonbonded interactions (for example, through the use of anisotropic united atoms[14,36,37]) and through the use of alternate forms for the torsional potential, has not been considered here.

The new method itself is not restricted to systems of fixed bond lengths and angles. A fully flexible implementation of the algorithm is straightforward. Constraints have been employed in this work to enable direct comparisons with past work.

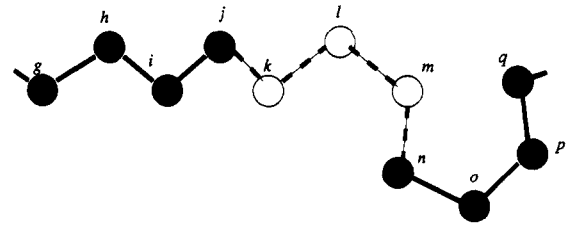

Figure 1. Geometry of a trimer $\{klm\}$ in a chain of prescribed bond lengths and angles. See text for details.

3. Monte Carlo Moves

Two new Monte Carlo moves are introduced in this section. The first of these effects a change in connectivity by constructing a trimer *bridge* between a chain end and an interior segment of another chain and excising one of the trimers neighboring the bridged interior atom. The second move is akin to the *concerted rotation*,[23] with a simplified iterative implementation thereof. Both of these moves proceed by solving the geometric problem of determining the coordinates of a trimer that bridges two spatially prespecified dimers.

In the simulations of volumetric behavior described in section 6, the new moves of this section are combined with reptations and volume fluctuations. For the purpose of simulating specific molecular weight distributions, the reptation move has been modified to allow for monomers to be transferred from one chain to another. In other respects, the reptation moves are essentially identical to those in earlier simulation work on polymer melts.[18,19,23]

3.1. The Geometric Bridge. Figure 1 depicts an internal trimer $\{k,l,m\}$ along a polymer chain. The position of this trimer is, of course, completely specified by the Cartesian coordinates of its constituent atoms, i.e. $\{\mathbf{r}_k, \mathbf{r}_l, \mathbf{r}_m\}$. Alternatively, the trimer is specified by the four bond lengths and five bond angles that fix it with respect to the rest of the chain—$\{l_{ijk}, l_{kl}, l_{lm}, l_{mn}, \theta_{ijk}, \theta_{jkl}, \theta_{klm}, \theta_{lmn}, \theta_{mno}\}$. The bond angles in conjunction with the bond lengths fix the distances between all pairs of atoms separated by two bonds along the chain, so that this *constraint* representation of the trimer may be simplified further to $\{l_{ijk}, l_{kl}, l_{lm}, l_{mn}, l_{ik}, l_{jl}, l_{km}, l_{ln}, l_{mo}\}$.

The Cartesian and constraint representations are linked by a set of nine equations of the form

$$(\mathbf{r}_p - \mathbf{r}_q)^2 - l_{pq}^2 = 0 \qquad (1)$$

one for each constraint l_{pq}. When a good initial guess

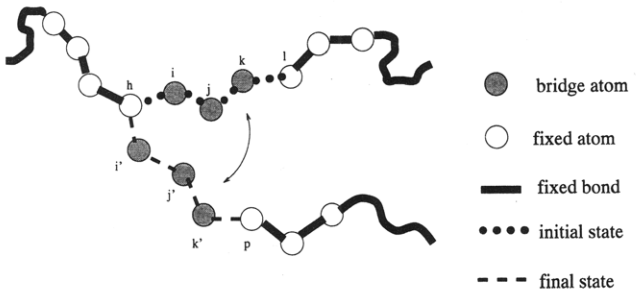

Figure 2. The *end-bridging* move. i,j,k and i',j',k' are the excised and rebridged trimers, respectively. p is the "attacking" chain end and l is the new chain end created by the move.

is available for the coordinates, these equations may readily be solved in an iterative Newton–Raphson procedure. This situation arises in intramolecular moves in which atoms j and n are rotated about bonds $\{hi\}$ and $\{op\}$, respectively, and then rebridged. In this circumstance, the initial coordinates of atoms k, l, and m form a reasonable initial guess for their final coordinates, especially when the torsional angles ϕ_{ghij} and ϕ_{qpon} are rotated by small amounts. The Newton–Raphson solution procedure has the advantage of being very simply implemented, but suffers from the difficulty that all solutions cannot be readily determined.

The nine equations above may also be reframed in terms of the six torsional angles around bonds ij, jk, kl, lm, mn, and no; this forms the basis of the *concerted rotation* of Dodd, Boone, and Theodorou.[23] More recently, a symmetric solution of the geometric bridge has been carried out.[24] In the symmetric solution, the trimer is specified by three variables: the two torsional angles ϕ_{ghij} and ϕ_{qpon}, and an angle ψ which defines the position of l on the circle of intersection of constraints l_{jl} and l_{ln}. The problem is reduced to a single equation in ψ which is solved for *all* solutions of the geometric bridge. This form of the solution is invoked in the implementation of the intermolecular move described later in this section.

It is useful to note that, in principle, infinite solutions are possible to the geometric bridge problem under special geometric conditions which would allow the trimer to rotate freely without distorting the bonds that connect it to the rest of the chain. These *crankshaft* geometries are precluded, however, by the values of bond length and angle in the model of section 2.

3.2. The End-Bridging Move. The end-bridging move alters the connectivity of the bulk polymer by *bridging* a chain end to an interior segment on another chain with a trimer. In parallel, one of the trimers adjoining the bridged internal segment is excised, preserving the total mass of the system. The move is depicted pictorially in Figure 2.

To facilitate the implementation of this move, special lists are maintained of candidates for bridging around each chain end. The criterion for inclusion in these "end-bridging lists" is that the candidate atom must be an internal segment of another chain within the all-trans bridging distance ($4l\cos(\theta/2)$) of a particular chain end, where l is the carbon–carbon bond length and θ is the supplement of the CCC bond angle. The number of bridgeable neighbors $N_{\text{bridge}}(p)$ of each chain end p in the system is continuously updated and enters into the acceptance criterion of the MC move.

The move is initiated by selecting a chain end p and one of its potential neighbors h from the list of $N_{\text{bridge}}(p)$ candidates at random (see Figure 2). Next, the geometric bridge procedure[24] is invoked to determine all geometrically admissible candidate configurations for the trimer bridge $\{i',j',k'\}$. These are subjected to two screening procedures: one based on the change in torsional energy and one based on hard-sphere overlaps of the bridge atoms with other atoms in the system. All solutions which would result in an increase in torsional energy greater than a prespecified value $\Delta\mathcal{V}_{\text{tor}}$ are discarded. Also discarded are all solutions that would result in overlaps with the positions of any unmoved atom in the system, based on the assignment of a hard-sphere diameter of σ_{HS} to each atom. These screening procedures are effective in efficiently culling the collection of geometrically valid solutions to a smaller, energetically viable set. Values for $\Delta\mathcal{V}_{\text{tor}}$ and σ_{HS} are selected heuristically to maximize the efficiency of the algorithm.

A prospective solution is chosen from the reduced set of feasible solutions, either at random, or weighting the solutions with the Boltzmann factor of the torsional energy $\mathcal{V}_{\text{tor}}$. This last procedure results in attempt probabilities for the forward and reverse moves given by

$$\alpha_{\text{select}}(m\rightarrow n) = \frac{\exp(-\mathcal{V}_{\text{tor}}(n)/k_{\text{B}}T)}{\sum_{n'=1}^{N^{(n)}} \exp(-\mathcal{V}_{\text{tor}}(n')/k_{\text{B}}T)} \tag{2}$$

$$\alpha_{\text{select}}(n\rightarrow m) = \frac{\exp(-\mathcal{V}_{\text{tor}}(m)/k_{\text{B}}T)}{\sum_{m'=1}^{N^{(m)}} \exp(-\mathcal{V}_{\text{tor}}(m')/k_{\text{B}}T)} \tag{3}$$

In eqs 2 and 3, m and n stand for the initial and final configurations of the system. $N^{(n)}$ and $N^{(m)}$ are the numbers of energetically viable solutions for the forward and reverse moves, respectively, determined at the end of the screening procedure defined above. Implicit in the geometric solution procedure is a transformation of coordinates from the Cartesian or dihedral to the *constraint* variables. This transformation is non-metric-preserving and calls into effect Jacobians that relate differential volume elements in the two coordinate systems. The need for such Jacobians has been elucidated in earlier work,[23] in which the recipe for their computation has also been discussed. For a molecular model with constant and equal skeletal bond lengths and bond angles, the Jacobians to be used in the end-bridging move differ only slightly from those of the concerted rotation;[23] the difference arises from the fact that in the concerted rotation, only *one* of the atoms neighboring the bridge trimer is displaced, whereas in this case *all* the coordinates of the heptamer centered at the bridge need to be considered together. The resulting form for the Jacobian for a heptamer numbered from 0 to 6 is[24]

$$J = \left|\frac{\mathbf{u}_6\cdot\mathbf{e}_3}{\det(\mathbf{B})}\right| \tag{4}$$

where $\mathbf{B}$ is the following 5×5 matrix:[23]

$$B = \begin{bmatrix} (\mathbf{u}_1\times\mathbf{r}_{51}) & (\mathbf{u}_2\times\mathbf{r}_{52}) & (\mathbf{u}_3\times\mathbf{r}_{53}) & (\mathbf{u}_4\times\mathbf{r}_{54}) & \mathbf{0} \\ (\mathbf{u}_1\times\mathbf{u}_6)\cdot\mathbf{e}_1 & (\mathbf{u}_2\times\mathbf{u}_6)\cdot\mathbf{e}_1 & (\mathbf{u}_3\times\mathbf{u}_6)\cdot\mathbf{e}_1 & (\mathbf{u}_4\times\mathbf{u}_6)\cdot\mathbf{e}_1 & (\mathbf{u}_5\times\mathbf{u}_6)\cdot\mathbf{e}_1 \\ (\mathbf{u}_1\times\mathbf{u}_6)\cdot\mathbf{e}_2 & (\mathbf{u}_2\times\mathbf{u}_6)\cdot\mathbf{e}_2 & (\mathbf{u}_3\times\mathbf{u}_6)\cdot\mathbf{e}_2 & (\mathbf{u}_4\times\mathbf{u}_6)\cdot\mathbf{e}_2 & (\mathbf{u}_5\times\mathbf{u}_6)\cdot\mathbf{e}_2 \end{bmatrix} \tag{5}$$

In the above, $\mathbf{u}_1$ to $\mathbf{u}_6$ are unit vectors along the six bonds of the heptamer, and $\mathbf{e}_1$ to $\mathbf{e}_3$ are the unit vectors

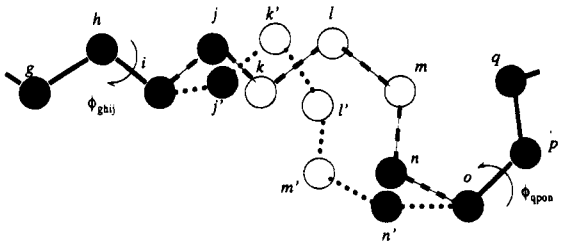

Figure 3. The *intramolecular rebridging* move. Atoms k, l, and m represent the initial coordinates of the bridge trimer; j and n are their neighbors in the original state. j' and n' are the coordinates of j and n after being rotated about bonds hi and po, respectively. k', l', and m' are the positions of the *rebridged* trimer.

of the global Cartesian coordinate system. To within a multiplicative constant, J in eq 4 equals the ratio of a volume element in Cartesian coordinate space to the corresponding volume element in constraint variable space.[24]

The computation of the nonbonded energies of the initial (m) and final (n) states forms the next stage in the implementation of the end-bridging move. The acceptance criterion must take into account the probability of selection of a given bridge site, the probability of selecting one of the multiple screened solutions at that site, the Jacobians of transformation from constraint to Cartesian coordinates in the initial and final states, and the composite energies of the initial and final states:

$$P(m\rightarrow n) = \min\left[1, \frac{\frac{1}{N_{\text{bridge}}(n\rightarrow m)}\alpha_{\text{select}}(n\rightarrow m)\exp\left(-\frac{\mathcal{V}(n)}{k_{\text{B}}T}\right)J(n)}{\frac{1}{N_{\text{bridge}}(m\rightarrow n)}\alpha_{\text{select}}(m\rightarrow n)\exp\left(-\frac{\mathcal{V}(m)}{k_{\text{B}}T}\right)J(m)}\right] \quad (6)$$

The evaluation of this acceptance criterion requires attempting the reverse move, complete with screening and weighting procedures. It is this symmetry in the use of the screening that renders the move microscopically reversible with arbitrarily selected values for σ_{HS} and $\Delta\mathcal{V}_{\text{tor}}$. In the simulations reported in this work, σ_{HS} has been set to 3.2 Å and $\Delta\mathcal{V}_{\text{tor}}$ to 3.5 kcal/mol.

3.3. The Intramolecular Rebridging Move. This move is analogous to the *concerted rotation*.[23,25] It induces local thermal fluctuations in the polymer, which in turn enhance the effectiveness of the end-bridging move by efficiently sampling fluctuations in the environment around the chain ends. The move is initiated by selecting at random an internal trimer $\{klm\}$ in the polymer. The two atoms neighboring this trimer, j and n (see Figure 3) are then displaced by rotating the torsional angles ϕ_{ghij} and ϕ_{qpon} by amounts randomly selected within prespecified bounds $(-\delta\phi_{\max}, \delta\phi_{\max})$.

Next, the system of nine constraint equations (1) is solved in an iterative Newton–Raphson procedure, with Gauss elimination being used to solve the linear system at each step. The procedure is repeated until convergence or up to a prespecified maximum of $N_{\max}$ steps. If a geometrically viable solution is found, a solution of the *reverse* move is attempted in an identical Newton–Raphson procedure. The move is rejected if the reverse move does not converge or if it converges to a solution other than the original coordinates of $\{k, l, m\}$. This ensures the microscopic reversibility of the move. Finally, the energies of the initial and final states ($\mathcal{V}(m)$ and $\mathcal{V}(n)$) are computed, as are the Jacobians of transformation $J(m)$ and $J(n)$. These Jacobians are necessitated by the implicit change of coordinates from those of the atoms ($\mathbf{r}_k$, $\mathbf{r}_l$, $\mathbf{r}_m$) to those of the constraints $\{l_{jk}, l_{kl}, l_{lm}, l_{mn}, l_{ik}, l_{jl}, l_{km}, l_{ln}, l_{mo}\}$; as pointed out in section 3.2, the rebridging move employs the latter. $J(m)$ and $J(n)$ represent ratios of volume elements in Cartesian space to volume elements in constraint space. In Appendix A, the essentials of the Newton–Raphson procedure are outlined; the computation of the Jacobians is shown to be facilitated by the form of the Gauss-eliminated Newton–Raphson matrix at convergence.

The acceptance probability of the move is

$$P(m\rightarrow n) = \min\left[1, \frac{\exp\left(-\frac{\mathcal{V}(n)}{k_{\text{B}}T}\right)J(n)}{\exp\left(-\frac{\mathcal{V}(m)}{k_{\text{B}}T}\right)J(m)}\right] \quad (7)$$

It is interesting to note that, unlike in the concerted rotation[23] and the end-bridging move, the intramolecular rebridging move described here locates only *one* geometric solution to the bridge. However, microscopic reversibility is enforced *explicitly* in this case, by rejecting all moves for which the reverse does not re-create the original configuration. A similar solution for the end-bridging move has not been attempted for lack of a convenient guess with which to initiate the iterative Newton–Raphson procedure.

4. Polydispersity

4.1. The [*NnPTμ] Ensemble for the Simulation of Polydisperse Polymers.** The Monte Carlo moves introduced in the previous section have the effect of inducing fluctuations in the chain length distribution. The resulting polydisperse systems can be thought of as multicomponent mixtures with the components differing from one another only in degree of polymerization. The statistical mechanics of polydisperse atomic fluids have been described by Briano and Glandt;[32] here, the analogous situation for mixtures of chain molecules of differing length is considered. Although the molecular weight distribution can change from realization to realization of the system in the end-bridging MC simulation, the *average* distribution may be controlled by specifying its conjugate variables, the spectrum of chemical potentials.

To facilitate simulations of polydisperse polymers, we have chosen a *semigrand* [*NnPTμ**] ensemble that specifies the total number of monomers n, the total number of chains in the system N, the system temperature T, the pressure P, and a reduced chemical potential spectrum μ^*, defined below.

A convenient starting point for developing the [*NnPTμ**] ensemble is the differential Helmholtz energy of a mixture of m components:

$$\mathrm{d}A = -S\,\mathrm{d}T - P\,\mathrm{d}V + \sum_{k=1}^{m}\mu_k\,\mathrm{d}N_k \quad (8)$$

which is linked to statistical mechanics by the relation

$$A(V,T,N_1,N_2,\ldots,N_m) = -k_{\text{B}}T\ln Q(V,T,N_1,N_2,\ldots,N_m) \quad (9)$$

$Q(V,T,N_1,N_2,\ldots,N_m)$ is the canonical partition function

for an m-component system:

$$Q(V,T,N_1,N_2,...,N_m) = \frac{1}{N_1!N_2!...N_m!}\frac{1}{\Lambda^{3n}}Z(V,T,N_1,N_2,...,N_m) \quad (10)$$

where

$$Z(V,T,N_1,N_2,...,N_m) = \int d^{3n}r \exp[-\beta \mathcal{V}(\mathbf{r}_1,...,\mathbf{r}_n)] \quad (11)$$

In the above, N_i stands for the number of i-mer chains in the system. $Z(V,T,N_1,N_2,...,N_m)$ is the classical configurational integral, Λ ($=h^2/2\pi m k_B T$) is the mer thermal wavelength, and $n = \sum_{k=1}^{m} kN_k$ is the total number of mers.

Selecting an arbitrary pair of components of lengths (i, j) as *reference* species, N_i and N_j are eliminated in favor of the total number of monomers n and the total number of chains $N = \sum_{k=1}^{m} N_k$:

$$dA = -S\,dT - P\,dV + \sum_{\substack{k=1\\k\neq i,j}}^{m} \mu_k^*\,dN_k + \mu^{(n)}\,dn + \mu^{(N)}\,dN \quad (12)$$

where

$$\mu_k^* = \mu_k - \left(\frac{k-i}{j-i}\right)\mu_j - \left(\frac{k-j}{i-j}\right)\mu_i \quad (13)$$

$$\mu^{(n)} = \frac{\mu_i - \mu_j}{i-j} \quad (14)$$

$$\mu^{(N)} = \frac{i\mu_j - j\mu_i}{i-j} \quad (15)$$

Legendre-transforming the above equation with respect to $\{N_k,\ k \neq (i, j)\}$ and the volume V, the natural thermodynamic potential for the variables of interest $(NnPT\mu^*)$ is obtained:[40]

$$Y = A - \sum_{\substack{k=1\\k\neq i,j}}^{m} \mu_k^* N_k + PV \quad (16)$$

$$dY = -S\,dT + V\,dP - \sum_{\substack{k=1\\k\neq i,j}}^{m} N_k\,d\mu_k^* + \mu^{(n)}\,dn + \mu^{(N)}\,dN \quad (17)$$

Y is related to a partition function $\tilde{Y}$ as

$$Y = -k_B T \ln \tilde{Y} \quad (18)$$

where[41]

$$\tilde{Y}[N,n,P,T,\mu^*] = \sum_{\{N_1,N_2,...,N_m\}} \exp[\beta \sum_{\substack{k=1\\k\neq i,j}}^{m} \mu_k^* N_k]\frac{1}{V_0}\int_0^\infty dV \exp(-\beta PV)Q(V,T,N_1,...,N_m) \quad (19)$$

In eq 19, summation over chain lengths is limited to those distributions for which

$$\sum_{k=1}^{m} N_k = N \quad (20)$$

$$\sum_{k=1}^{m} kN_k = n \quad (21)$$

Equation 19 defines the probability density in connectivity and configuration space that is sampled in our simulations. In these simulations monomers are treated as distinguishable entities, while exchanging the identity of two chains of the same length does not create a new configuration. Thus, the probability density sampled is

$$\varrho^{NnPT\mu^*}(V,\mathbf{r}_1,...,\mathbf{r}_n;\text{connectivity}) = \text{const} \times \exp[\beta \sum_{\substack{k=1\\k\neq i,j}}^{m} \mu_k^* N_k - \beta PV - \beta \mathcal{V}(\mathbf{r}_1,\mathbf{r}_2,...,\mathbf{r}_n;\text{connectivity})] \quad (22)$$

4.2. Limiting Molecular Weight Distributions. Simulations in the $[NnPT\mu^*]$ ensemble yield a molecular weight distribution that depends on the spectrum of chemical potentials, μ^*. The relationship between the chemical potential spectrum and the chain length distribution is greatly simplified in cases wherein the configurational integral in eq 11 depends on the monomer density and number-averaged molecular weight, but not on the details of the distribution, i.e., if

$$Z(V,T,N_1,N_2,...,N_m) = Z(V,T,N,n) \quad (23)$$

When this condition is satisfied, the molecular weight distribution is related to the chemical potential spectrum μ^* solely by combinatoric considerations and does not depend on the energetics of the system. Condition (23) would hold exactly in systems of noninteracting unperturbed chains (no intermolecular, no nonbonded intramolecular interactions), where Z can be reduced to a product of Z's of individual chains, each depending exponentially on the chain length. One would expect that this condition would also hold in systems with realistic potentials, provided short-chain species were absent, under which circumstance the properties of the melt would depend only on the monomer density and the density of chain ends. The extent to which the analysis of this section is valid depends on the extent to which the configurational integral $Z(V,T,N_1,N_2,...,N_m)$ varies with the specifics of the chain length distribution within the bounds imposed upon its fluctuations. The predictions of this section are tested against the results of simulations of realistic models of polyethylene in section 6.

When N and n are large, a maximum term approximation on $\ln \tilde{Y}$ subject to the constraints (20) and (21) may be invoked to map the distribution of chemical potentials onto the corresponding distribution of chain lengths. Using Stirling's approximation for the logarithms of factorial terms, this yields $(m - 2)$ equations of the form

$$\ln N_k = \beta\mu_k^* + \xi + \psi k \qquad (k = 1,...,m,\ k \neq i,j) \quad (24)$$

where ξ and ψ are Lagrange multipliers corresponding to the two constraints (20) and (21). These equations

simplify to

$$N_k = cy^k \exp(\beta\mu_k^*) \qquad (k = 1,...,m, k \neq i,j) \tag{25}$$

Analogously, the reference species are governed by the following relations:

$$N_i = cy^i \tag{26}$$

$$N_j = cy^j \tag{27}$$

The m equations above are substituted into the constraints (20) and (21) to solve for the constants c and y, thereby yielding the entire distribution.

4.2.1. The Most Probable Distribution. This distribution is commonly observed in the products of condensation polymerization. The number fraction of an oligomeric species is an exponentially decaying function of chain length.

Under the condition that eq 23 is satisfied, this distribution results if the reduced chemical potential spectrum is set to zero for all chain lengths. A truncated form of the most probable distribution results if a minimum chain length is imposed, i.e., if the chemical potentials are specified as

$$\mu_k^* = \begin{cases} -\infty & \text{for } k < k_{\min}; \\ 0 & \text{for } k \geq k_{\min}, k \neq i, k \neq j \text{ with } k_{\min} \leq i < j \end{cases} \tag{28}$$

which has the solution

$$N_k = \begin{cases} 0, & \text{for } 1 \leq k < k_{\min} \\ cy^k, & \text{for } k_{\min} \leq k \end{cases} \tag{29}$$

In conjunction with the two constraints (20) and (21), a truncated exponential distribution results:

$$\frac{N_k}{N} = \frac{1}{X - k_{\min} + 1}\left[\frac{X - k_{\min}}{X - k_{\min} + 1}\right]^{k-k_{\min}}, \qquad k \geq k_{\min} \tag{30}$$

and $N_k/N = 0$ otherwise, where $X = n/N$ is the number-averaged degree of polymerization.

4.2.2. The Uniform Distribution. It is also straightforward to generate a uniform distribution of chain lengths of width $(2l + 1)$, centered at the number-averaged degree of polymerization, X. The chemical potential specification for this case is

$$\mu_k^* = \begin{cases} -\infty & \text{for } k < X - 1 \text{ or } k > X + l \\ 0, & \text{for } X - l \leq k \leq X + l, k \neq i, k \neq j, \\ & \text{with } X - l \leq i < j \leq X + l \end{cases} \tag{31}$$

Again, the solution for the N_k is of the form

$$N_k = cy^k, \qquad k = X - l, X - l + 1, ..., X + l - 1, X + l \tag{32}$$

and $N_k = 0$ otherwise. The two constraints (20) and (21) are satisfied by the solution $y = 1$, and the resulting distribution is

$$\frac{N_k}{N} = \frac{1}{2l + 1}, \qquad \text{for } X - l \leq k \leq X + l \tag{33}$$

while $N_k/N = 0$ otherwise.

4.2.3. The Gaussian Distribution. A Gaussian distribution may also be used to control the deviation from monodispersity. In the athermal case, this distribution results if the reduced chemical potential is quadratic in the chain length:

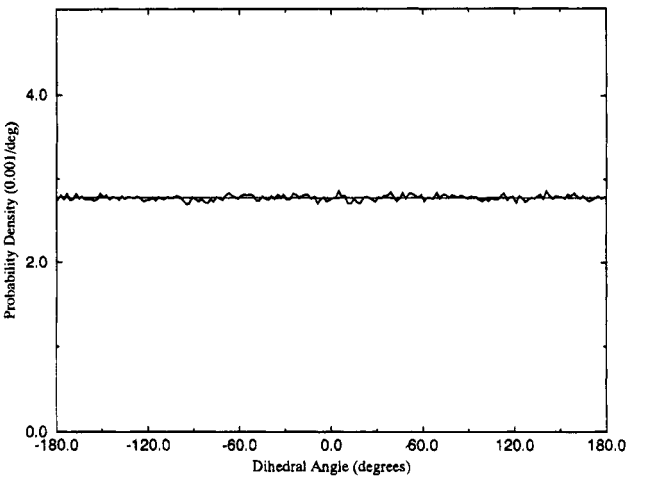

Figure 4. Dihedral angle distribution of a phantom chain in a simulation consisting of reptations and intramolecular rebridges in the ratio 1:1.

$$\mu_k^* = \begin{cases} \psi[l^2 - (X - k)^2], & \text{for } X - l < k < X + l \\ -\infty, & \text{for } k < X - l \text{ or } k > X + l \end{cases} \tag{34}$$

The chain length distribution obtained by substitution into the set of $(2l + 1)$ equations (25), (26), and (27) is

$$N_k = c'y^k \exp[-\beta\psi(X - k)^2], \qquad X - l \leq k \leq X + l \tag{35}$$

The constraints (20) and (21) are satisfied by $y = 1$, and the resulting distribution is a truncated Gaussian:

$$\frac{N_k}{N} = \frac{\exp[-\beta\psi(k - X)^2]}{\sum_{k'=-l}^{l} \exp[-\beta\psi k'^2]}, \qquad \text{for } X - l \leq k \leq X + l \tag{36}$$

and $N_k/N = 0$ otherwise. For $\beta\psi l^2 \gg 1$, $\beta\psi \ll 1$, the distribution is well approximated by

$$\frac{N_k}{N} = \left(\frac{\beta\psi}{\pi}\right)^{1/2} \exp[-\beta\psi(k - X)^2] \tag{37}$$

5. Tests of Monte Carlo Moves

The acceptance criteria listed for the two new Monte Carlo moves (eqs 6 and 7), if correct, should lead to the correct asymptotic distribution for any chain molecular system. It is most convenient to test these moves on systems of *phantom* chains, in which torsional and nonbonded energetics are excluded. In this circumstance, the torsional angles along the chains should uniformly sample the interval $(-\pi,\pi)$. This test has been seen to detect subtle shortcomings in the microscopic reversibility of a simulation algorithm, such as would be caused by the omission of Jacobians of transformation or by an incorrect accounting of the multiplicity of solutions.[23]

Figure 4 shows the distribution of the dihedral angle of a phantom chain resulting from a Monte Carlo simulation that employs intramolecular rebridges and reptations in the ratio 1:1. The simulation was conducted on a single chain of C_{24} starting from an all-trans configuration, for a total of two million MC moves. Figure 5 shows the resulting distribution for the same

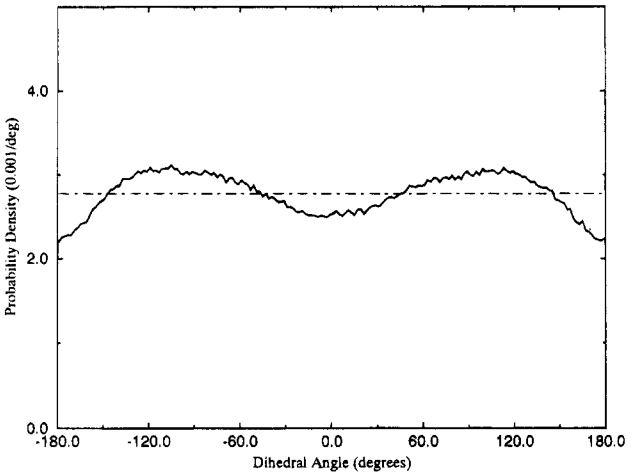

Figure 5. Dihedral angle distribution of a phantom chain in a simulation consisting of reptations and intramolecular rebridges in the ratio 1:1. Jacobians of transformation were omitted from the acceptance criterion of the intramolecular rebridges.

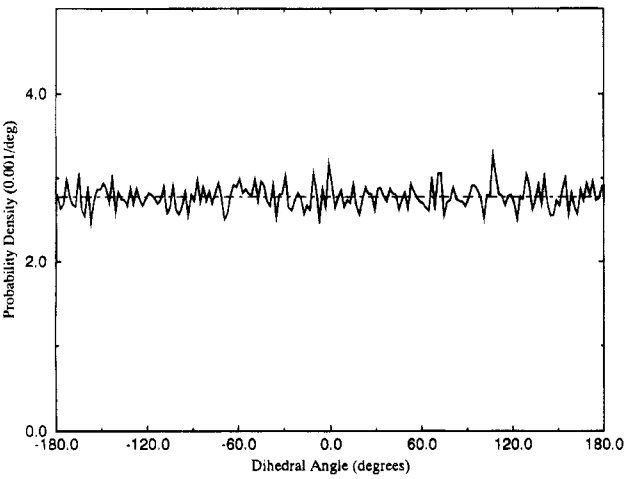

Figure 6. Dihedral angle distribution of phantom chains in a simulation consisting of reptations and end-bridges in the ratio 1:1.

set of moves and the same duration of simulation, but with an acceptance criterion that omitted the Jacobians of transformation. Clearly, the simulations that employ the criterion of eq 7 do sample the space of the dihedral angle uniformly, as expected; the simulations that ignore the Jacobians are incorrect.

Similarly, Figures 6 and 7 display the results of an identical test for the end-bridging move, in which it is combined with reptations in the ratio 1:1. A periodic system of 32 phantom chains of C_{24} was simulated. The initial state of the system was an equilibrated melt with full energetics; its structure was thus far removed from the uniform torsional angle distribution, exhibiting strong peaks at the *trans* ($\phi = 0$) and *gauche* ($\phi = \pm\pi/3$) states. The simulation was run for 700 000 moves in all. All reptations in the phantom chain simulation are accepted. Although only about 20% of the end-bridges were accepted, this corresponded to a ratio of approximately 1:1 in torsions altered by the two moves. This is because each end-bridging move alters six torsional angles, while each reptation resets only one angle. Again, the results show that the acceptance criterion of eq 6 yields the appropriate uniform distribution of dihedral angles (Figure 6), while the omission of Jacobians ($J(m)$ and $J(n)$) and the correct attempt probability terms ($\alpha_{\text{select}}(m\rightarrow n)$, $\alpha_{\text{select}}(n\rightarrow m)$, $N_{\text{bridge}}(m\rightarrow n)$, $N_{\text{bridge}}(n\rightarrow m)$) from the acceptance criterion results in

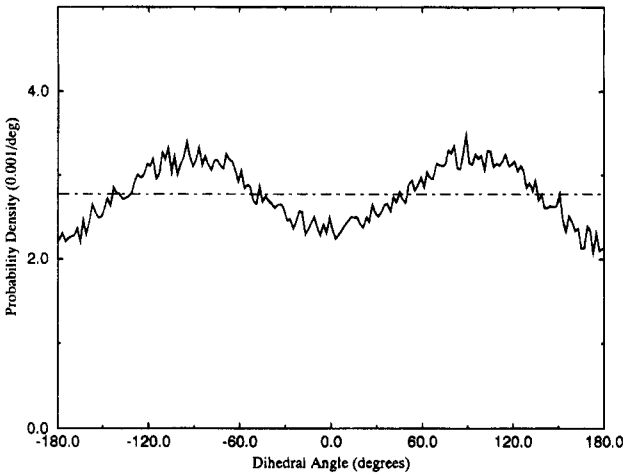

Figure 7. Dihedral angle distribution of phantom chains in a simulation consisting of reptations and end-bridges in the ratio 1:1. Jacobians of transformation and asymmetric attempt probabilities arising from the multiplicity of bridge solutions were omitted from the acceptance criterion of the end-bridges.

systematic deviations from uniform sampling (Figure 7).

Further tests of the validity of the new simulation algorithm lie in its predictions of structural and volumetric properties for realistic polymer melts. These are discussed in the next section.

6. Results

In this section, the results of simulations of realistic atomistically detailed polydisperse melts of polyethylene are described. This allows for a comparison of the structural and volumetric properties predicted by the new simulation technique with those from earlier simulations. Next, tests are made of the mappings between the chain length distribution and the spectrum of reduced chemical potentials derived in section 4.2. Finally, the efficiency of the new algorithm in equilibrating the polymer melt is assessed.

Two sets of simulations were performed: one with 32 chains of average degree of polymerization $X = 24$, and the other with 10 chains and $X = 78$. Both sets of simulations were carried out at a temperature of 450 K and at a pressure of 1 atm. The molecular weight distribution, unless otherwise specified, was a uniform distribution of chain lengths between ($X/2$) and ($3X/2$) for C_{78}, and a uniform distribution between ($3X/4$) and ($5X/4$) in the case of C_{24}. This corresponds to a polydispersity index (M_w/M_n) of 1.085 in the former melt and 1.024 in the latter. The MC moves employed were reptations, end-rotations, intramolecular rebridges, end-bridges, and volume fluctuations in the ratio {12:12:96:79:1}.

Melts of C_{24} are readily equilibrated by a variety of simulation techniques; the first set therefore allows for comparisons with reliably estimated properties. The second set of simulations is particularly significant because all other simulation methods in current use have proved inadequate to the task of thermally equilibrating melts of chain length greater than C_{70}.[15,16] The ability to equilibrate chains of C_{78} in a reasonable amount of computation time would represent a significant step toward the reliable treatment of long-chain, entangled polymeric melts.

6.1. Melt Structure and Chain Conformation Characteristics. The structure of polymeric melts may be thought of as having two related aspects: the

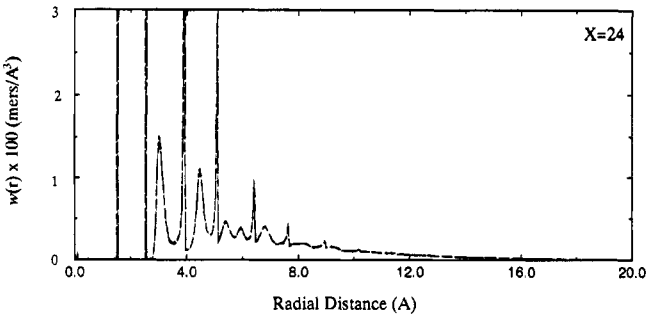

Figure 8. Intramolecular pair density function $\omega(r)$ for C_{24}, in units of 10^{-2} mers/Å^3: dotted curve, result of bulk ($NnPT\mu^*$) Monte Carlo simulation; dashed curve, result from fast sampling of continuous unperturbed chains.

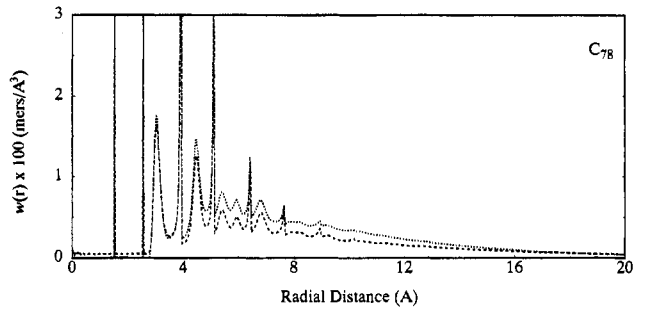

Figure 9. Intramolecular pair density function $\omega(r)$ for C_{78}, in units of 10^{-2} mers/Å^3: dotted curve, result of bulk (NPT) concerted rotation Monte Carlo simulation; dashed curve, result from fast sampling of continuous unperturbed chains.

intramolecular structure, as defined by the intrachain pair density function $\omega(r)$, and the intermolecular packing, as expressed most directly in the bulk density. According to the random coil hypothesis, the intrachain structure of polymer chains in the bulk is determined on the average by short-range interactions, with long-range interactions being screened out by interactions with other chains. An explicit test of this hypothesis is the comparison of chain conformations in the equilibrated melt with those of *continuous unperturbed chains*.[25] Continuous unperturbed chains (CUCs) are isolated chains incorporating only local interactions.[24,39] In the case of tetracosane (C_{24}), it has been found in earlier work[25] that such unperturbed chains, including only the torsional potential and the pentane-effect nonbonded interaction between atoms separated by four bonds along the chain, have the same structure as chains in the melt, providing a direct verification of the random coil hypothesis. This finding is verified with the new simulation technique as applied to C_{24} in Figure 8, in which the pair density functions for the melt and CUCs are seen to be almost indistinguishable. This constitutes a more refined test of the algorithm than the tests on phantom chains in section 5. The structure of the unperturbed chains was determined from rapid Monte Carlo simulations with interchain reptation moves and employing the same chemical potential spectrum as in the simulations of the melt.

Interestingly, it was found in the same earlier study[25] that the structure of longer CUCs (C_{78}) differed from that of chains in the melt as obtained in concerted rotation MC simulations (see Figure 9). It was also determined that the melt structure in those simulations had not reached equilibrium, despite exceedingly long simulation runs. The simulations reported in this work were initiated from the final structures of that study. Within a few million MC moves (a few thousand cycles) with the new algorithm, chains in the melt were found to converge to the intrachain structure of the unperturbed chains (Figure 10). The discrepancy between the two at very short distances is expected: it arises from occurrences of overlaps between segments far separated along the unperturbed chains. Besides demonstrating the validity of the new simulation method, Figure 10 provides powerful evidence that the simulations efficiently sample the conformations of the polymer in a dense long-chain melt at all length scales.

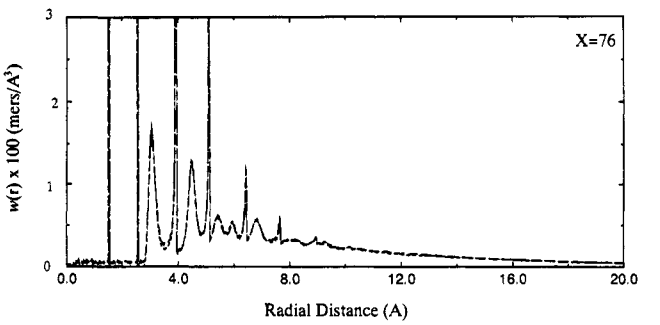

Figure 10. Intramolecular pair density function $\omega(r)$ for C_{78}, in units of 10^{-2} mers/Å^3: dotted curve, result of bulk ($NnPT\mu^*$) Monte Carlo simulation; dashed curve, result from fast sampling of continuous unperturbed chains.

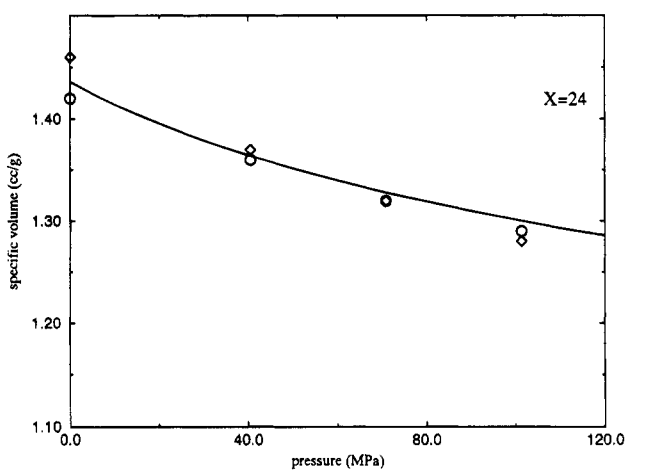

Figure 11. Variation of volume with pressure for a melt of C_{24}. The curve represents the experimental data; the circles are the results of the new end-bridge simulations, and the diamonds represent the simulation results of the *concerted rotation* algorithm.

The PVT predictions of polymer simulations are also of interest. In Figure 11 the results of the new simulation technique are compared with the experimental volume–pressure curve for a melt of C_{24} at 450 K[38] and with previous simulation results based on the same potentials.[25] The new predictions are found to be in good agreement with earlier simulation results and with experiment.[38] Interestingly, the polydispersity inherent in the new results has little impact on PVT behavior. This is probably explained by the (M_w/M_n) ratio of 1.024 in the simulations being very close to monodispersity.

In Figure 12, the same comparison is made for the melt of C_{78}. Here, it is seen that the results of the new simulations are uniformly lower than both the experimental curve and the results of previous simulations based on the same model.[25] This cannot be attributed to a lack of equilibration in the current simulation, because the intrachain structure is seen to have completely converged. Although the discrepancy is small (~2%), it is interesting to note that a similar phenomenon has been observed in dynamic simulations of alkane melts,[14] in which it has been traced to the inadequacy of the potential for methylene–methylene interactions. It was found that UA potentials calibrated

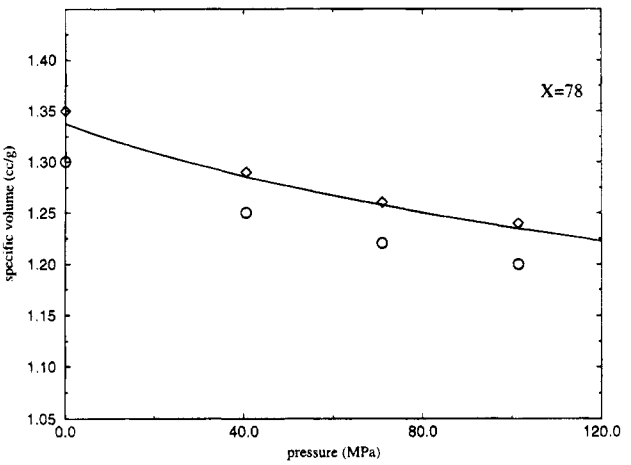

Figure 12. Variation of volume with pressure for a melt of C_{78}. The curve represents the experimental data; the circles are the results of the new end-bridge simulations, and the diamonds represent the simulation results of the *concerted rotation* algorithm.

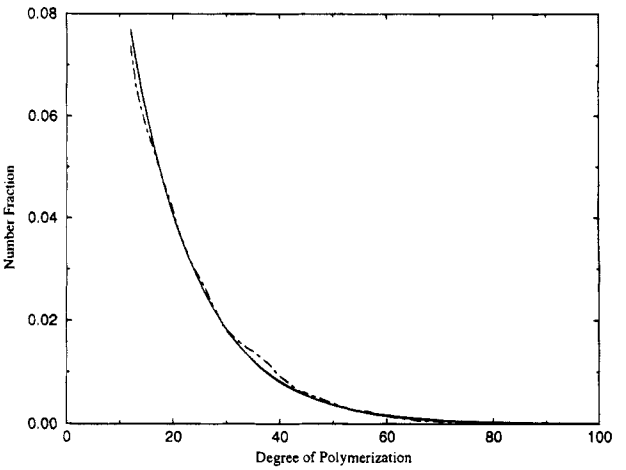

Figure 13. A truncated most probable chain length distribution: solid curve, theoretical result; dashed curve, results from an ($NnPT\mu^*$) simulation. The average chain length is 24 and the minimum allowed length is 12. The simulation system contains 32 chains.

to give the correct volume at short chain lengths tend to underpredict the specific volume of melts of longer chains. This strongly suggests that the discrepancy with experimental volumetric behavior seen in Figure 12 arises from shortcomings of the UA Lennard-Jones potential. The previous concerted rotation simulation results might well have been affected by their incomplete equilibration. The issue of recalibrating the methylene–methylene nonbonded interaction, such as through the use of anisotropic united atom (AUA) potentials,[14,36,37] has not been addressed here.

6.2. Molecular Weight Distributions. One of the most interesting features of the new simulation method is the flexibility it allows in controlling the polydispersity of the polymer. This feature could, in fact, be used in conjunction with any other MC simulation method, providing a ready recipe for the extension of those methods to polydisperse polymers. In section 4.2., several limiting chain length distributions are mapped analytically onto spectra of the reduced chemical potential. Although these mappings are strictly valid only in systems of noninteracting unperturbed chains, the deviation from these results in realistic polymer melts is expected to be small when extremely short species are disallowed. The extent of this deviation may be simply thought of as arising from the relative effect of energetics and combinatorics on the molecular weight distribution. Since the effect of energetics on chain structure is essentially local, it is unlikely to have an impact on the chain length distribution of a mixture of moderate to long chains. This is directly verified in three sets of simulations of C_{24} in Figures 13, 14, and 15, representing a truncated "most probable" distribution, a truncated Gaussian distribution, and a uniform distribution of chain lengths, respectively. In the first case, species shorter than 12 segments were disallowed. In the latter two cases, only species between 18 and 30 segments in length were permitted. The *untruncated* Gaussian curve that would be formed by extending the curves of Figure 14 to $\pm\infty$ would have a standard deviation of 5. To facilitate an efficient sampling of chain length fluctuations, a modified reptation move was employed, in which ends could be transferred from one chain to another. In each case, no more than 5 million MC moves were needed to converge to the distributions displayed. The results demonstrate that the [$NnPT\mu^*$] ensemble is extremely effective in simulating prespecified chain length distributions.

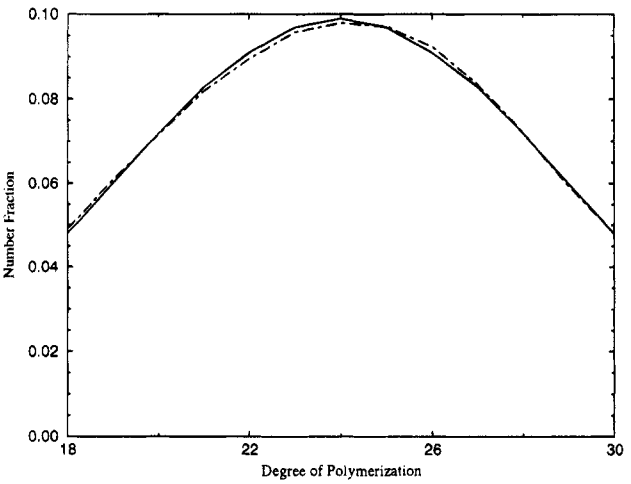

Figure 14. A truncated Gaussian chain length distribution: solid curve, theoretical result; dashed curve, results from an ($NnPT\mu^*$) simulation. The average chain length is 24 and the minimum allowed length is 18. The simulation system contains 32 chains and the standard deviation of the *untruncated* curve is 5.

6.3. Efficiency. The central objective in developing the new polydisperse polymer simulation method was to enable simulations of melts of reasonably long geometrically detailed chains within accessible computation times. It is essential that this aspect of the simulation method be evaluated for the longest chain lengths simulated. To this end, two measures have been employed in assessing the sampling efficiency of the algorithm. The first is the rate of diffusion of the chain center of mass. This is displayed for the ($NnPT\mu^*$) simulations of C_{78} in Figure 16. The simulations were carried out restricting the polydispersity index (M_w/M_n) to 1.085, with a uniform distribution of chain lengths ranging from 39 to 117 segments. The average mean-squared end-to-end distance of the C_{78} chain is about 1200 Å^2; thus, the chains diffuse by several times their dimensions in 4000 cycles of the simulation. A cycle consists of one MC attempt per degree of freedom in the system. The computation time required for a simulation of 4000 cycles is of the order of 1.5 h on a CRAY C-90 computer, which represents only a modest computational expense. In contrast, a wide range of dynamic and MC methods have been determined to be insufficient for the thermal equilibration of melts of chains of this length.[15,16]

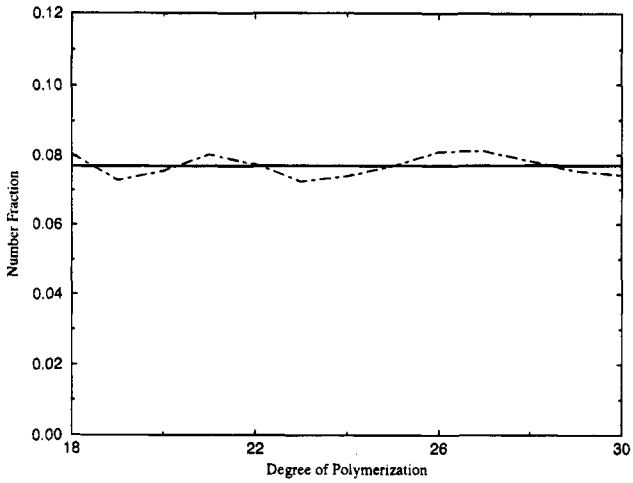

Figure 15. A uniform chain length distribution: solid line, theoretical result; dashed curve, results from an ($NnPT\mu^*$) simulation. The average chain length is 24 and the allowed range of chain lengths is 18–30. The simulated system contains 32 chains.

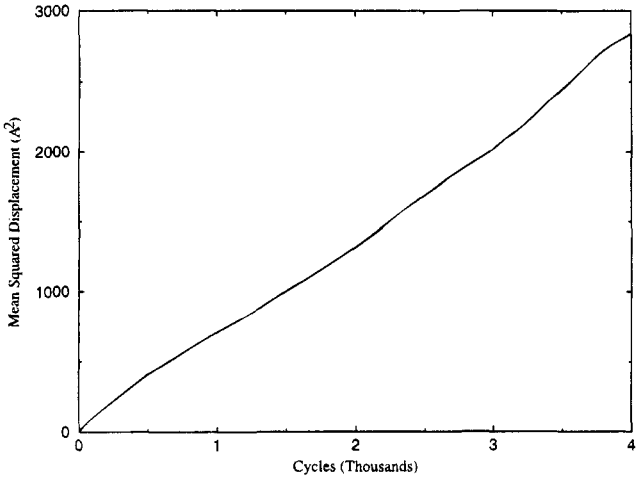

Figure 16. Mean-squared displacement vs Monte Carlo cycles for a 10-chain C_{78} system at 450 K and 0.1 MPa.

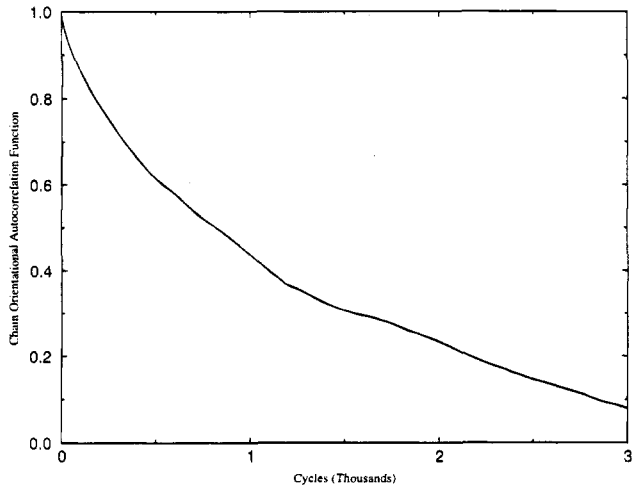

Figure 17. Autocorrelation function for the end-to-end vector, $\langle \mathbf{u}(0)\cdot\mathbf{u}(t)\rangle$, vs Monte Carlo cycles for a 10-chain C_{78} system at 450 K and 0.1 MPa.

The efficiency of the algorithm may also be measured in terms of the rate of evolution of the end-to-end vector of the chains, as represented by the autocorrelation function $\langle \mathbf{u}(0)\cdot\mathbf{u}(t)\rangle$, where $\mathbf{u}$ is the unit vector along the end-to-end vector of the polymer. As seen in Figure 17, this autocorrelation function decays rather rapidly for the C_{78} simulations. In fact, within 3000 cycles, the chains lose almost all memory of their initial orientation. This is further evidence that the simulations robustly sample the conformation space of the polymer in the dense melt. It is interesting to note that this efficiency persists even at reasonably low overall polydispersities such as in the systems simulated in the present work and for chains of moderate length. Part of the reason for this phenomenon is that, in most other methods, thermal equilibration proceeds by means of a diffusion of the chain essentially along its contours, thereby requiring an equilibration time that rises very rapidly with chain length; on the other hand, the end-bridging method proceeds by the diffusion of connectivity relationships, which do not scale in the same manner.

Studies of the relationships among simulation efficiency, chain length, and system size for the end-bridging method are currently in progress. It appears that the simulation may be thought of as introducing structural fluctuations on disparate length scales through the complementary action of its constituent moves: concerted rotations and reptations sample the local thermal fluctuations of the chains, while end-bridges rapidly reconfigure the long-range structure by transferring subchains of moderate length from molecule to molecule. The new method holds promise, therefore, for simulation studies of longer, entangled polymer systems.

Acknowledgment. We are indebted to E. I. du Pont de Nemours for a generous gift in support of this work and to the San Diego Computer Center for a grant of computer time.

Appendix A. Solution Procedure and Jacobians of Transformation in the Intramolecular Rebridging Move

As outlined in section 3.3, the intramolecular rebridging move employs an iterative Newton–Raphson solution of the nine constraint equations (1):

$$\sigma_{pq} = (\mathbf{r}_p - \mathbf{r}_q)^2 - l_{pq}^2 = 0 \tag{38}$$

where σ_{pq} is the constraint linking atoms p and q. The complete set of nine constraints $\boldsymbol{\sigma}$ is (see Figure 3)

$$\boldsymbol{\sigma} = \{\sigma_{jk}, \sigma_{kl}, \sigma_{lm}, \sigma_{mn}, \sigma_{ik}, \sigma_{jl}, \sigma_{km}, \sigma_{ln}, \sigma_{mo}\} \tag{39}$$

Thus, at each step of the procedure, the matrix

$$\mathbf{C} = \begin{bmatrix} \frac{\partial\sigma_{jk}}{\partial r_{k1}} & \frac{\partial\sigma_{jk}}{\partial r_{k2}} & \frac{\partial\sigma_{jk}}{\partial r_{k3}} & \frac{\partial\sigma_{jk}}{\partial r_{l1}} & \frac{\partial\sigma_{jk}}{\partial r_{l2}} & \frac{\partial\sigma_{jk}}{\partial r_{l3}} & \frac{\partial\sigma_{jk}}{\partial r_{m1}} & \frac{\partial\sigma_{jk}}{\partial r_{m2}} & \frac{\partial\sigma_{jk}}{\partial r_{m3}} \\ \frac{\partial\sigma_{kl}}{\partial r_{k1}} & \frac{\partial\sigma_{kl}}{\partial r_{k2}} & \frac{\partial\sigma_{kl}}{\partial r_{k3}} & \frac{\partial\sigma_{kl}}{\partial r_{l1}} & \frac{\partial\sigma_{kl}}{\partial r_{l2}} & \frac{\partial\sigma_{kl}}{\partial r_{l3}} & \frac{\partial\sigma_{kl}}{\partial r_{m1}} & \frac{\partial\sigma_{kl}}{\partial r_{m2}} & \frac{\partial\sigma_{kl}}{\partial r_{m3}} \\ \vdots & & & \vdots & & & \vdots & & \\ \frac{\partial\sigma_{mo}}{\partial r_{k1}} & \frac{\partial\sigma_{mo}}{\partial r_{k2}} & \frac{\partial\sigma_{mo}}{\partial r_{k3}} & \frac{\partial\sigma_{mo}}{\partial r_{l1}} & \frac{\partial\sigma_{mo}}{\partial r_{l2}} & \frac{\partial\sigma_{mo}}{\partial r_{l3}} & \frac{\partial\sigma_{mo}}{\partial r_{m1}} & \frac{\partial\sigma_{mo}}{\partial r_{m2}} & \frac{\partial\sigma_{mo}}{\partial r_{m3}} \end{bmatrix} \tag{40}$$

which contains the derivatives of the constraints σ_{pq} with respect to the atomic coordinates of the bridge trimer, is evaluated. The increment to the bridge trimer coordinates is determined by solving the linear system

$$\mathbf{C}\Delta\mathbf{r}_{\text{bridge}} = -\boldsymbol{\sigma} \tag{41}$$

The procedure is repeated until the constraints are

satisfied to within a prespecified tolerance ϵ. At convergence, the matrix **C** holds the derivatives of the *constraint* coordinates of the bridge with respect to its Cartesian coordinates, for state (n) in the forward move and for state (m) in the reverse move. Thus, the inverse determinant of this matrix directly yields the Jacobians of transformation $J(m)$ and $J(n)$ to be considered in the acceptance criterion, eq 7. The computation of this determinant is further simplified when the linear system (41) is solved by Gauss elimination, which yields an upper triangular matrix **C′** that has a determinant identical to that of **C**. The Jacobians may therefore be evaluated conveniently as

$$J = (\prod_{i=1}^{9} \mathbf{C}'_{ii})^{-1} \tag{42}$$

References and Notes

(1) See papers in *Adv. Polym. Sci.* **1994**, *116*.
(2) Roe, R.-J., Ed. *Computer Simulation of Polymers*; Prentice-Hall: Englewood Cliffs, NJ, 1991.
(3) Boyd, R. H.; Gee, R. H.; Han, J.; Jin, Y. *Macromolecules* **1994**, *27*, 7781.
(4) Matsuda, T.; Smith, G. D.; Winkler, R. G.; Yoon, D. Y. *Macromolecules* **1995**, *28*, 165.
(5) Smith, G. D.; Yoon, D. Y.; Zhu, W.; Ediger, M. D. *Macromolecules* **1994**, *27*, 5563.
(6) Smith, G. D.; Yoon, D. Y. *J. Chem. Phys.* **1993**, *100*, 649.
(7) Rigby, D.; Roe, R.-J. In *Computer Simulation of Polymers*; Roe, R.-J., Ed.; Prentice-Hall: Englewood Cliffs, NJ, 1991; p 79.
(8) Han, J.; Gee, R. H.; Boyd, R. H. *Macromolecules* **1994**, *27*, 7781.
(9) Rigby, D.; Roe, R.-J. *J. Chem. Phys.* **1987**, *87*, 7285.
(10) Rigby, D.; Roe, R.-J. *J. Chem. Phys.* **1988**, *89*, 5280.
(11) Han, J.; Boyd, R. H. *Macromolecules* **1994**, *27*, 5365.
(12) Pant, P. V. K.; Boyd, R. H. *Macromolecules* **1993**, *26*, 679.
(13) Müller-Plathe, F. *J. Chem. Phys.* **1993**, *98*, 9895.
(14) Pant, P. V. K.; Boyd, R. H. *J. Chem. Phys.* **1993**, *99*, 597.
(15) Forrest, B. M.; Suger, U. W. *J. Chem. Phys.* **1994**, *101*, 2616.
(16) Leontidis, E.; de Pablo, J. J.; Laso, M.; Suter, U. W. *Adv. Polym. Sci.* **1994**, *116*, 283.
(17) Allen, M. P.; Tildesley, D. J. *Computer Simulation of Liquids*; Clarendon: Oxford, 1987; p 116.
(18) Vacatello, M.; Avitabile, G.; Corradini, P.; Tuzi, A. *J. Chem. Phys.* **1980**, *73*, 548.
(19) Boyd, R. H. *Macromolecules* **1989**, *22*, 2477.
(20) Siepmann, J. I. *Mol. Phys.* **1990**, *70*, 1145.
(21) de Pablo, J. J.; Laso, M.; Suter, U. W. *J. Chem. Phys.* **1992**, *96*, 2395.
(22) Siepmann, J. I.; Frenkel, D. *Mol. Phys.* **1992**, *75*, 59.
(23) Dodd, L. R.; Boone, T. D.; Theodorou, D. N. *Mol. Phys.* **1993**, *78*, 961.
(24) Boone, T. D.; Theodorou, D. N., in preparation.
(25) Dodd, L. R.; Theodorou, D. N. *Adv. Polym. Sci.* **1994**, *116*, 249.
(26) Duane, S.; Kennedy, A. D.; Pendleton, B. J.; Roweth, D. *Phys. Lett. B* **1987**, *195*, 216.
(27) Forrest, B. M.; Suter, U. W. *Mol. Phys.* **1994**, *82*, 393.
(28) Olaj, O. F.; Lantschbauer, W. *Makromol. Chem., Rapid Commun.* **1982**, *3*, 847.
(29) Mansfield, M. L. *J. Chem. Phys.* **1982**, *77*, 1554.
(30) Madden, W. G. *J. Chem. Phys.* **1987**, *87*, 1405; **1988**, *88*, 3934.
(31) Lastoskie, C. M.; Madden, W. G. In *Computer Simulation of Polymers*; Roe, R.-J., Ed.; Prentice-Hall: Englewood Cliffs, NJ, 1991; p 233.
(32) Briano, J. G.; Glandt, E. D. *J. Chem. Phys.* **1984**, *80*, 3336.
(33) Kofke, D. A.; Glandt, E. D. *Mol. Phys.* **1988**, *64*, 1105.
(34) Pant, P. V. K.; Theodorou, D. N. *Polym. Prepr. (Am. Chem. Soc., Div. Polym. Chem.)* **1994**, *35*, 165.
(35) Ryckaert, J.-P.; Bellemans, A. *Chem. Phys. Lett.* **1975**, *30*, 123.
(36) Toxvaerd, S. *J. Chem. Phys.* **1990**, *93*, 4290.
(37) Padilla, P.; Toxvaerd, S. *J. Chem. Phys.* **1991**, *94*, 5650.
(38) Dee, G. T.; Ougizawa, T.; Walsh, D. J. *Polymer* **1992**, *33*, 3462.
(39) Vacatello, M.; Yoon, D. Y. *Macromolecules* **1992**, *25*, 2502.
(40) Modell, M.; Reid, R. C. *Thermodynamics and Its Applications*, 2nd ed.; Prentice-Hall: Englewood Cliffs, NJ, 1983; Chapter 5.
(41) For an explanation of the correspondence between transformation of ensembles and Legendre transforms in the fundamental equation of thermodynamics, see: Chandler, D. *Introduction to Modern Statistical Mechanics*; Oxford University Press: New York, 1987; p 62–71.

MA950521K